

Effects of a shelterbelt on road dust dispersion



Y. Mao^a, J.D. Wilson^{a,*}, J. Kort^b

^aDepartment of Earth & Atmospheric Sciences, University of Alberta, Edmonton, Canada T6G 2E3

^bAgriculture & Agri-Food Canada, Indian Head, Saskatchewan, Canada S0G 2K0

HIGHLIGHTS

- Studied impact of a two-row tree shelterbelt on dust plumes off a gravel road during windy conditions.
- Shelterbelt did not reduce the aerial concentration of PM₁₀ particles.
- Reasonable agreement of measured and simulated transects of mean wind speed.
- Disagreement between measured and modelled dust plumes.
- Higher fidelity treatment of one or more aspects of the problem needed.

ARTICLE INFO

Article history:

Received 24 November 2012

Received in revised form

3 July 2013

Accepted 5 July 2013

Keywords:

Air quality

Airborne particulate

Dust control

Environment

PM₁₀

Road dust

Shelterbelts

Windbreaks

ABSTRACT

The impact of a roadside shelterbelt on the downwind concentration of road dust raised by a passing vehicle was investigated experimentally, and by numerical modelling. With or without the shelterbelt, the gravel dust plume, as measured some 60 m or more downwind from the road, was dominated by small particles (most frequent diameter $\approx 6 \mu\text{m}$) whose gravitational settling velocity was negligible compared to the turbulent velocity scale (i.e. friction velocity). The time-averaged concentration of these small particles was not lower in the lee of the shelterbelt than in a nearby, unsheltered area downwind of the road. Standard formulae for spheres in an airstream negotiating obstacles suggest such fine particles may pass through the shelterbelt on the bleed flow with little likelihood of interception and entrainment, because their small inertial time constant mandates that they accelerate with the wind, deviating around foliage. Numerical simulations of the experiment are consistent in some respects with what was observed, and suggest that the shelterbelt may increase the fraction of fine particles remaining airborne one minute after their injection at the road.

Crown Copyright © 2013 Published by Elsevier Ltd. All rights reserved.

1. Introduction

Dust raised from unpaved rural roads represents a nuisance and potentially a pulmonary health risk for those regularly inhaling a fine fraction liable to enter and remain in their lungs. Factors affecting the amount of dust raised off an unpaved road include vehicle type, weight and speed, and the condition and composition of the road surface. Spraying rural roads with water, oil or other dust suppressants (e.g. Gillies et al., 1999) is a common intervention to control dust, but it would be useful to establish more definitively the potential effectiveness of roadside vegetation in scrubbing dust from the airstream, and/or enhancing the rate of plume dilution and deposition. Earlier studies have quantified the dust emission

factor (mass per vehicle kilometre travelled, kg VKT^{-1}) under normal or controlled traffic conditions, by using artificial tracer techniques or by adopting an atmospheric dispersion model that allows a relation to be obtained between a measured dust concentration and an (implied) emission rate (Claiborn et al., 1995; Kantamaneni et al., 1996). Other work has used the integrated horizontal flux (IHF) method to investigate the downwind fate of a road dust cloud. Working over an open desert surface (roughness length $z_0 = 0.005 \text{ m}$) Etyemezian et al. (2004) determined that the loss of PM₁₀ particles (diameter $d \leq 10 \mu\text{m}$) between the unpaved road and a point 100 m downwind was less than 9.5%, while in contrast Veranth et al. (2003) found that over 85% of PM₁₀ dust particles had vanished from the airstream over a comparable fetch of much rougher surface (specifically an artificial “urban canopy,” composed of shipping containers).

A slow rate of loss of PM₁₀ aerosols from an airstream on open ground might be expected, given the small terminal velocity w_g of

* Corresponding author.

E-mail address: jaydee.uu@ualberta.ca (J.D. Wilson).

Table 1

Particle terminal velocity w_g , particle inertial time constant $\tau \equiv g^{-1}w_g$, and normalized impaction conductance g_p/U versus particle diameter d . Impaction conductance is given for two values of the air speed U around foliage. Assumptions: air pressure 93 kPa and temperature 25 °C; characteristic dimension of foliage $d_c = 0.05$ m; kinematic viscosity of air $\nu = 1.55 \times 10^{-5}$ m² s⁻¹; dust particle density $\rho_p = 1522$ kg m⁻³ (Note: in LS simulations the Stokes number St was evaluated with U given by the instantaneous particle speed).

$d, \mu\text{m}$	$w_g, \text{m s}^{-1}$	τ, s	$g_p/U, U = 1 \text{ m s}^{-1}$	$g_p/U, U = 5 \text{ m s}^{-1}$
1	4.9e-5	5.0e-6	6.3e-8	1.6e-6
2	1.97e-4	2.0e-5	1.1e-6	2.3e-5
6	0.0018	1.8e-4	8.0e-5	1.9e-3
10	0.0049	5.0e-4	6.0e-4	0.012
20	0.020	2.0e-3	8.3e-3	0.11
50	0.12	1.2e-2	0.15	0.58
100	0.49	5.0e-2	0.51	0.86

PM₁₀ particles (Table 1 gives theoretical values of w_g), but the character of the downwind surface and its vegetation must play a role by virtue of their control over the near ground profiles of mean wind speed and turbulence, potentially multiplying the opportunities for particles to come in close contact with and deposit onto surfaces (the ground, or foliage), and delaying the rate of advection of dust downwind. Pardyjak et al. (2008) have developed a model to compute the fate of a particulate plume rising from a road and encountering a uniform canopy of vegetation. The present paper focuses on the efficacy of shelterbelts, i.e. narrow roadside belts of trees, which have been considered a possible means of abating the problem of nuisance road dust (Steffens et al., 2012). We shall describe an experiment and related numerical modelling that, taken together, suggest shelterbelts (of the type and in the configuration studied) may not substantially ameliorate the problem of wind-borne road dust in the PM₁₀ category.

2. Experiment

Dust samplers and cup anemometers were arranged on (geographic) east–west transects perpendicular to a long, straight, rural gravel road, parallel to which and 60 m downwind (eastward) ran a two-row shelterbelt (see Figs. 1 and 2). “Shelter” transects ran through (or above) and downwind of the shelterbelt, while “reference” transects 100 m away traversed an open (*nominally* unsheltered) area at the south end of the shelterbelt. The objective was to measure and interpret differences between the dust distributions in the open and in the lee of the shelterbelt. To this end during suitable meteorological conditions — a strong westerly wind, a dry road — dust was raised by making repeated passes of a 3/4 ton truck, driven at about 80 km h⁻¹ and in as consistent a manner as could be managed. The interval between consecutive passes (S–N, N–S, S–N...) was two minutes, and each experiment consisted of twenty such passes over 40 min. Five experiments were executed on five different days, but here the discussion is restricted to two experiments performed during strong winds and (consequently) weak thermal stratification¹ (see Table 2).

The shelterbelt, located at (a constant) longitude -103.99237° and spanning latitude range 50.58810° – 50.59335° (i.e. 583 m oriented north–south geographic), consisted of a row of green ash (*Fraxinus pennsylvanica* Marsh.) on the western side and a row of Scots pine (*Pinus sylvestris* L.). The overall cross-section of the shelterbelt was $W \approx 4.7$ m, and the mean height $H \approx 10$ m. In the

discussion to follow the origin of the east–west (i.e. x or x/H) coordinate is taken to lie at the centre of the shelterbelt such that the road is centred at $x = -60$ m ($x/H = -6$), and the north–south coordinate y runs parallel to the road with its origin $y = 0$ at the south end of the shelterbelt. Upwind of the shelterbelt stretched a crop of peas whose continuity was interrupted by the road with shallow ditches on either side, while downwind of the shelterbelt ($x > 0$) stood a crop of flax. Both upwind and downwind, the canopy height was $h_c \approx 0.4$ m. The reference transects were located at $y = -25$ m ($y/H = -2.5$), that is, 25 m south of the south end of the shelterbelt, and they bisected a cut break (of about 50 m width) that spanned from the south end of the shelterbelt to an abandoned farmyard (still farther south, and not represented on Fig. 1) growing scrub and short trees of irregular height. This small separation ($2.5H$) between the south end of the shelterbelt and the reference transects implies that with increasing downwind distance x/H the broadening wakes of the shelterbelt and the farmyard scrub must have impinged on (and modified) the airstream carrying dust plumes downwind along the reference transect. Measured mean wind speeds (shown later, Fig. 3) confirm this disturbance.

The transects were instrumented (see Fig. 1) at three east–west locations $x/H = (0.75, 5, 10)$ and two heights $z/H = (0.2, 1.2)$. Rotorod-type spore counters (viz. 2 mm square-section rods, rotating at 2400 RPM on a 2 cm radius) provided size-discriminated 40 min mean concentrations $\bar{c}_k(x, y, z)$, where k labels particle diameter bins of width 1 μm and spanning $1 \mu\text{m} \leq d \leq 100 \mu\text{m}$; a size-dependent collection efficiency was assumed in converting from the Rotorod particle count, performed automatically using Image Pro software (Media Cybernetics, Inc., Rockville, Maryland), to the implied aerial concentration. Co-located Casella Microdust Pro sensors (Model 176000A, Casella CEL, Buffalo, New York) provided 40 min time series of size-aggregated dust mass concentration $c(x, y, z, t)$ spanning 20 vehicle passes, and from those twenty realizations it was possible to approximate for each Casella sensor an ensemble mean concentration transient $\langle c \rangle$. Individual correction factors for the Casella instruments were assigned on the basis of an intercomparison with all instruments exposed close together during test passes of the vehicle.

Table 2 gives the micrometeorological conditions during the two experiments discussed here. A three-dimensional sonic anemometer at height $z_s = 2$ m and standing at $x/H = -3$ on the reference transect provided the mean wind vector $\bar{u}_i \equiv (\bar{u}, \bar{v}, \bar{w})$, the mean kinematic sensible heat flux density vector $\bar{u}_i T_i'$ and all components of the Reynolds stress tensor $\bar{u}_i' u_j'$. From that information the friction velocity (u_*) and Obukhov length (L) were computed as

$$u_* = \sqrt[4]{\bar{u}'\bar{u}'^2 + \bar{v}'\bar{v}'^2}, \quad (1)$$

$$L = \frac{-u_*^3 T_0}{g k_v \bar{w}' T_i'}, \quad (2)$$

where $k_v = 0.4$ is the von Karman constant, g is gravitational acceleration and T_0 is the mean Kelvin temperature. Roughness length was inferred by best-fitting the Paulson (1970) mean wind profile, using the Monin–Obukhov universal functions recommended by Dyer and Bradley (1982), to the mean wind speed, friction velocity and heat flux density provided by the sonic anemometer. The reference wind speed $U_r = \bar{u}(12 \text{ m})$ cited in Table 2 was computed by extrapolation using the resulting mean wind profile.

3. Numerical simulations

A preliminary analysis of the experiments established that such data as it had been possible to gather would not suffice to

¹ In this respect (and several others) the present work differs from that of Steffens et al. (2012), whose focus was the fate of sub-micron particles raised by ambient traffic on a paved urban motorway during a period of very light winds (mean wind speed $\bar{u} = 0.57$ m s⁻¹ at $z = 3$ m).

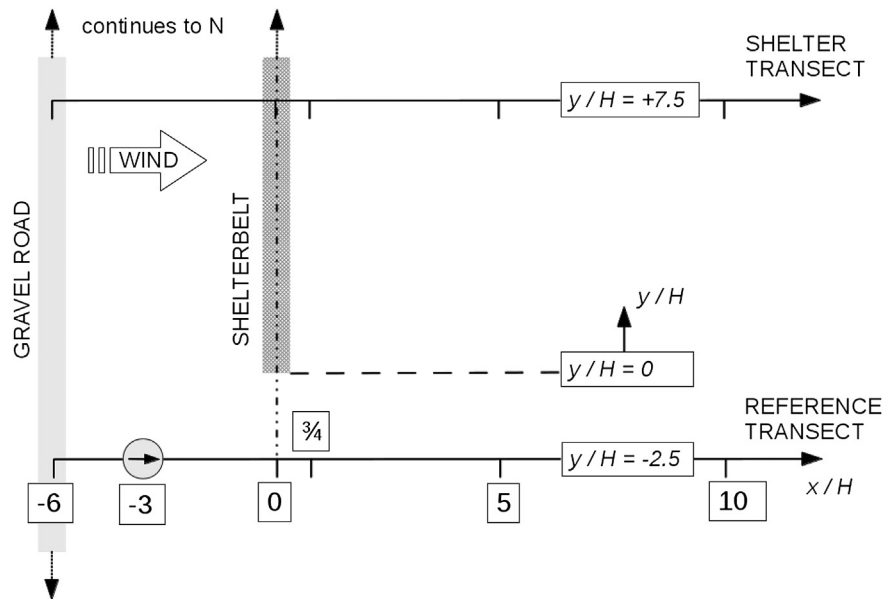


Fig. 1. Schematic of the site, giving alongwind coordinates (x/H , where $H = 10$ m is the height of the shelterbelt) of the road ($x/H = -6$), sonic anemometer (circular symbol at $x/H = -3$), shelterbelt ($x/H = 0$) and dust samplers ($x/H = 3/4, 5, 10$). The windbreak continued towards the north (top of diagram), the road continued north and south. The shelter transect and the reference transect were separated by distance $\Delta y/H = 10$. (Not drawn to scale.)

determine unambiguously the impact of the shelterbelt on dust clouds. To complement the field data we carried out comparative numerical simulations of the motion of dust clouds in undisturbed winds, and in a synthetic shelter flow that has been matched (approximately) to the conditions of the experiment. The numerical simulations idealize the problem, however they should capture at least *qualitatively* the twofold impact of the shelterbelt — its disturbance of the flow field carrying the passing dust clouds, and its potential role as a particle filter. Comparable simulations, treating the interaction of a plume of glass beads with a belt of maize, have been described by Bouvet et al. (2007).

Dust particle trajectories were computed using a Lagrangian stochastic (LS) model, adopting the “settling sticky fluid element” paradigm as described by Wilson (2000). A gravitational settling velocity w_g appropriate to dust particles of given size was superposed on a velocity series that otherwise (and but for a suitable

reduction of the particle velocity autocorrelation time scale) would have been appropriate to a fluid element, and trajectories were terminated with probability P upon contact with the ground ($z = z_0$, $P = 1$) or with shelterbelt foliage (P computed as function of particle diameter, wind speed etc.; further details below). For simulations of dust dispersion along the reference transect the horizontal inhomogeneity alluded to above (see also Fig. 3) was neglected, and velocity statistics needed to drive the LS model were provided by adopting Monin–Obukhov profiles for height extrapolation of statistics determined by the sonic anemometer. For simulations of trajectories around and through the shelterbelt, two-dimensional fields of the required velocity statistics were obtained by solving Reynolds-averaged momentum equations with second-order turbulence closure, using the methods described by Wilson (1985, 2004).

3.1. Disturbed wind and turbulence field

The mean streamwise momentum equation appropriate to the problem is

$$\bar{u} \frac{\partial \bar{u}}{\partial x} + \bar{w} \frac{\partial \bar{u}}{\partial z} = -\frac{1}{\rho_0} \frac{\partial \bar{p}}{\partial x} - \frac{\partial \overline{u'^2}}{\partial x} - \frac{\partial \overline{u'w'}}{\partial z} - S_u \quad (3)$$

where \bar{p} is the mean pressure disturbance induced by the shelterbelt, ρ_0 is the mean air density, $\overline{u'^2}$ is the variance of the streamwise velocity and $\overline{u'w'}$ is the kinematic vertical flux of streamwise momentum (Reynolds stress). The final term on the right hand side of

Table 2

Summary of meteorological conditions for the near-neutral experiments. Friction velocity u_* , mean wind speed $z = 3$ upwind of the road at $z = 12$ m, Obukhov length L , mean wind direction β (270° for a west wind) and standard deviation σ_β of wind direction during the experiment.

Date	u_* , m s ⁻¹	U_r , m s ⁻¹	L , m	z_0 , m	β , deg	σ_β , deg
27/7/11	0.73	10.09	-184	0.0325	225	15.9
23/8/11	0.65	9.09	-106	0.0275	283	14.1



Fig. 2. View of the shelterbelt looking towards the WNW, roughly along the line of the reference (“unsheltered”) transect. The origin $y/H = 0$ of the north–south axis is at the south (left) end of the shelterbelt, and the reference transect lies along $y/H = -2.5$.

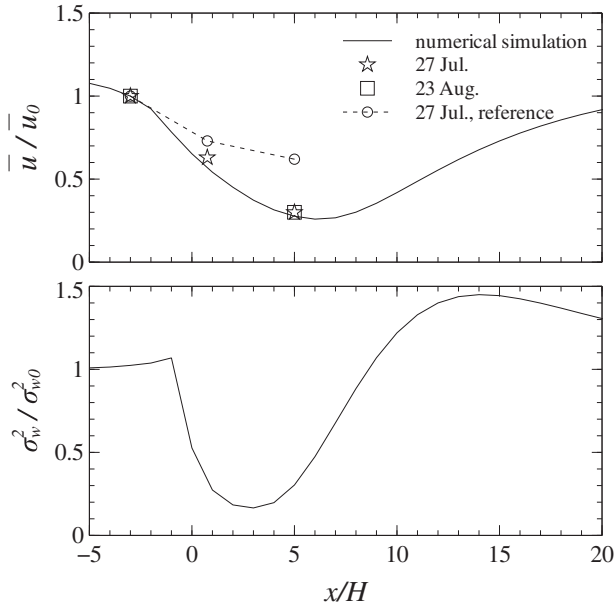


Fig. 3. Observed and simulated transects of relative mean wind speed \bar{u}/\bar{u}_0 (upper panel) and a simulated transect of the normalized vertical velocity variance σ_w^2/σ_{w0}^2 (lower panel) along $z/H = 0.2$ ($z = 2$ m) through a shelterbelt, \bar{u}_0 being the upstream (undisturbed) mean wind speed and σ_{w0}^2 the upstream vertical velocity variance at 2 m. Symbols give the observations at Indian Head, and lines are from a numerical solution of the Reynolds-averaged Navier–Stokes equations ($H/z_0 = 330$, $k_r = 2.5$; further details in text). The open circles on the upper panel register the relative mean wind speeds observed on the reference transect along $y/H = -2.5$, and as they decrease with increasing distance downwind, they show that this was not sufficiently far isolated from the influence of the shelterbelt. (Wind speeds on the reference transect not available on 23 Aug.)

Eq. (3) represents the rate of loss of streamwise momentum to the shelterbelt, and it was parameterized as

$$S_u = k_r \bar{u} \sqrt{\bar{u}^2 + \bar{w}^2} \delta(x-0) s(z-H) \approx k_r \bar{u} |\bar{u}| \delta(x-0) s(z-H), \quad (4)$$

where k_r is a (dimensionless) resistance coefficient. The interpretation of Eq. (4) is that a drag vector, proportional to $k_r(\bar{u}^2 + \bar{w}^2)$ and projected onto the x -axis by the factor $\bar{u}/\sqrt{\bar{u}^2 + \bar{w}^2}$, is localized to $x = 0$, $z \leq H$ by the product of the delta function $\delta(x-0)$ (with units m^{-1}) and a dimensionless unit step function $s(z-H)$. In other words, for the purpose of computing the wind field the Indian Head shelterbelt was treated as an infinitely thin porous barrier located at $x = 0$ (the middle of the actual shelterbelt). Please note that although by virtue of Eq. (4) the finite alongstream width of the shelterbelt was neglected for the purpose of the wind calculation, when computing dust particle trajectories in that wind field the shelterbelt was properly represented by a belt of (uniform) vegetation spanning $x = 0 \pm 2.35$ m.

The Indian Head shelter flow was simulated numerically by solving Eq. (3) and coupled equations (notably the corresponding vertical momentum equation, the continuity equation, and parameterized Reynolds-stress equations) using the second-order closure of Launder et al. (1975). Full details of the numerical procedure are provided by Wilson (1985). The computational domain covered $-20 \leq x/H \leq 120$, $z/H \leq 47$. At the inflow boundary the usual semi-logarithmic mean wind profile (Eq. (11)) was imposed; consistent with this, and because the “host (i.e. upwind) flow” could legitimately be approximated as a constant stress layer, the inflow profile of the turbulent kinetic energy dissipation rate (ϵ) was specified by Eq. (13), and all components of the Reynolds stress tensor were specified as being height-independent (in particular,

the normalized velocity standard deviations $\sigma_u/u^* = 1.7$, $\sigma_v/u^* = \sigma_w/u^* = 1.3$); these choices constitute the algebraic solution of the coupled equations for horizontally-homogeneous, neutrally-stratified and steady-state winds. Resolution along the streamwise coordinate was uniformly $\Delta x/H = 1$, while the vertical resolution was held at $\Delta z/H = 0.1$ for $z/H \leq 2$, and progressively coarsened aloft (again, it is crucial to be clear that it is the field of wind statistics whose spatial resolution is referred to here: when computing dust particle paths, much finer steps were used. Much higher computational resolution of the flow field could easily have been achieved. However for this work it was not necessary to achieve grid-independence in the flow calculation, because in effect all that was wanted was a best fit of the model to our very limited observations of mean wind speed. Wilson, 1985, showed that a streamwise resolution of $\Delta x/H = 1$ provides what is, for our purposes in this paper, an adequately detailed simulation of the mean wind transect for normal flow through a windbreak). The RANS (Reynolds-averaged Navier–Stokes) solution requires only two inputs, namely the ratio H/z_0 and the resistance coefficient k_r . The observations fix H/z_0 , and we have taken $H/z_0 = 330$. The resistance coefficient was treated as a tuneable parameter, and optimized by requiring that the numerical solution should best reproduce the observed three point transect of mean wind speed through the shelterbelt at $z/H = 0.2$. (As shown by Wilson, 1985, fractional mean wind reduction near a windbreak is essentially determined by k_r .)

Fig. 3 gives the computed fields of mean wind speed and vertical velocity variance along the shelter transect at height $z = 2$ m, for the case that $k_r = 2.5$ (the optimal value). Regarding mean wind speed, plotted as a relative wind speed (i.e. normalized on the value upwind in the approaching flow), by virtue of the freedom to assign k_r the model transect agrees well with that observed, which furthermore, and as is only to be expected, was consistent across these two near-neutral observation periods. The open circles on the upper panel of Fig. 3 give the transect of mean wind speed observed on Jul. 27 along the reference transect (corresponding observations for Aug. 23 are unavailable). The observed decay in wind speed with increasing x/H confirms what Fig. (2) suggests, namely that this transect was not sufficiently far isolated from the spreading wake of the shelterbelt to permit its being regarded as a transect characterizing unsheltered (undisturbed) roadside winds.

The lower panel of Fig. 3 indicates that the model generates the expected “quiet zone” of reduced turbulent kinetic energy in the near wake of the shelterbelt, and the zone of increased turbulence further downwind that is a consequence of the adverse pressure gradient and of the accentuated wind shear accompanying a jet of displaced air accelerating over the top of the shelterbelt. Observations are not available to compare with the computed velocity variance, but earlier studies indicate that the model replicates observed patterns fairly well (e.g. Bourdin and Wilson, 2008).

3.2. Further particulars of trajectory calculations

The methodology for the trajectory calculations is as given by Wilson et al. (2010), and only details specific to the present problem will be given. The LS model is driven by the gridded mean wind and turbulence fields provided by the RANS model (for the shelter transect), or by (gridded) Monin–Obukhov profiles (for the reference transect). It is assumed that symmetry prevails in the crosswind (y) direction, so that the ability of the LS model to discriminate gradients along y is not called into action.

The friction velocity and roughness length were fixed at $u^* = 0.7 \text{ m s}^{-1}$, $z_0 = 0.03 \text{ m}$, values closely representing the actual conditions of the experiment (see Table 2) and which correspond to a value of $U_r = 10.5 \text{ m s}^{-1}$ for the reference wind speed (i.e. wind speed at $z = 12 \text{ m}$, far away from the shelterbelt). To account for the

initial mixing of dust in the vehicle wake, particles were released at $t = 0$ at uniformly distributed random points within a “volume” surrounding the centre of the road, the choice $-6.15 \leq x/H \leq -5.85$, $z_0/H \leq z/H \leq 0.15$ providing best agreement between the observed concentration field and that reconstructed by the LS model. The gravitational settling velocity w_g was computed for each particle size class by adopting Stokes’ law

$$w_g = \frac{1}{18\nu} g d^2 \frac{\rho_p}{\rho}, \quad (5)$$

where ν is the kinematic viscosity of air, ρ is air density and ρ_p is the dust particle density, taken as $\rho_p = 1500 \text{ kg m}^{-3}$. Table 1 gives indicative values.

Dust entrapment by foliage was parameterized as follows. Mass conservation can be expressed

$$\frac{dc}{dt} = -\alpha g_p c, \quad (6)$$

where d/dt is the particle-following derivative, $\alpha [\text{m}^{-1}]$ the foliage area density and $g_p [\text{m s}^{-1}]$ the impaction conductance. Now supposing that a particle travels a streamwise distance Δx at speed U within the shelterbelt, the fractional change in dust concentration is

$$\frac{\Delta c}{c} = -\alpha \Delta x \frac{g_p}{U}, \quad (7)$$

which provides the probability of absorption. The ratio g_p/U of the impaction conductance to the air speed around foliage was evaluated for each particle size following Raupach et al. (2001) as

$$\frac{g_p}{U} = \left(\frac{\text{St}}{0.8 + \text{St}} \right)^2, \quad (8)$$

where the Stokes number

$$\text{St} = \frac{1}{9\nu} \frac{d^2 U \rho_p}{d_e \rho} \quad (9)$$

involves the instantaneous wind speed and a characteristic foliage dimension d_e , which we prescribed as $d_e = 0.05 \text{ m}$. Table 1 gives indicative values of g_p/U for several particle diameters.

The foliage area density α within a shelterbelt of (narrow) width W may be estimated (Wilson, 1985) from the approximation $k_r \approx 1/2c_d\alpha W$, where k_r is the apparent (effective) resistance coefficient and c_d is the foliage drag coefficient. For the Indian Head shelterbelt $W \approx 5 \text{ m}$ and from the optimal RANS simulation of the flow $k_r \approx 2.5$, so that $c_d\alpha \sim 1 \text{ m}^2 \text{ m}^{-3}$. The foliage drag coefficient is not known (Peltola et al., 1997, cite $c_d = 0.29$ for Scots pine). For the present calculations we prescribed $\alpha = 2 \text{ m}^2 \text{ m}^{-3}$, a choice that affects (only) the entrapment probability.

The time step for the computations was $\Delta t = 0.1\tau$, where τ is the velocity autocorrelation time scale along the trajectory. The latter was specified as

$$\tau = \frac{2\sigma_w^2(z)}{C_0\epsilon(z)} \frac{1}{\sqrt{1 + 2w_g/\sigma_w}} \quad (10)$$

where the σ_w^2 is the vertical velocity variance, ϵ is the turbulent kinetic energy dissipation rate and C_0 is a (nominally, universal) dimensionless constant evaluated here as $C_0 = 4.3$ (see Wilson et al., 2009). For the reference (unsheltered) flow, velocity

statistics were (a gridded representation of) those of a neutral surface layer, viz.

$$\bar{u} = \frac{u_*}{k_v} \ln \frac{z}{z_0}, \quad (11)$$

$$\sigma_{u,v,w} = (2, 2, 1.25)u_*, \quad (12)$$

$$\epsilon = \frac{u_*^3}{k_v z}, \quad (13)$$

while for the shelter flow computed non-uniform fields were provided by the RANS calculation.

The trajectory simulations were effectively two-dimensional in that the cross-wind (y) location of particles played no role. Suppose one wishes to determine the theoretical value for the mean concentration at a location with coordinates x_D, z_D (‘D’ for Detector) due to a continuous line source ($\text{kg m}^{-1} \text{ s}^{-1}$) having the same aggregate mean rate of emission per unit of distance along the road as occurred during the experiment. To that end one may introduce an infinitely long narrow strip of the $y-z$ plane, with depth Δz and centred on height x_D, z_D . One releases N_p particles sequentially (and independently) from the road (or in this case from randomly chosen points near the road). Each time a given particle crosses this strip it can be considered to reside within the (hypothetical) cross-section $\delta z \delta x$ ($\delta x \ll \delta z$) for a time equal to $\delta x/|U|$, where U is the alongwind velocity with which the plane is crossed (δx can be viewed as being infinitesimal). Let \bar{T}_R designate the mean residence time within $\delta z \delta x$, averaged over all particles. Then

$$\frac{\bar{c}}{Q} [\text{s m}^{-2}] \equiv \frac{\bar{T}_R}{\delta z \delta x} \quad (14)$$

is a normalized mean concentration (that is, ratio of mean concentration to source strength Q) due to this equivalent line source, where the units of \bar{c} are kg m^{-3} , and those of Q are $\text{kg m}^{-1} \text{ s}^{-1}$. In practice, rather than forming \bar{T}_R by summing increments $\delta x/|U|$ and ultimately dividing \bar{T}_R by δx , one simply increments a counter by the amount $1/|U|$ each time a particle crosses the detector strip, obviating need to introduce this imaginary thickness of the strip. For the calculations reported, the vertical resolution $\delta z = 0.2 \text{ m}$. Concentration *transients* were computed by time-resolving particle transits across the detector strip such that mean residence time $\bar{T}_R = \bar{T}_R(t)$, where t is time since a particle was released. Computed transients shown here provided 0.1 s resolution, but have been smoothed for display using a block average over $\pm 1 \text{ s}$. (As a point of clarification, please note that actual, physical source strengths are not needed in order to perform simulations, whose output is a concentration *per unit* of release.)

4. Results and discussion

Fig. 4 gives the observed transects of 40 min mean concentration provided by the Rotorod detectors, for two particle size classes. Small particles dominate the observed dust clouds at these locations, and most notably dust concentrations in the lee of the shelterbelt hardly differ from those on the reference transect. Fig. 5, from the Rotorod samplers on 27 July, shows that at all locations the dust size distribution was similar, and strongly peaked at about $6 \mu\text{m}$. The measurements do not establish whether this predominant particle size in the observed plumes represents the *emitted* size distribution from traffic on this road, for presumably (and as suggested by computations) larger dust particles had deposited to a greater degree from the flow before arriving at the samplers, the closest of which (at $x/H = 0.75$) lay almost 70 m downwind from the road.

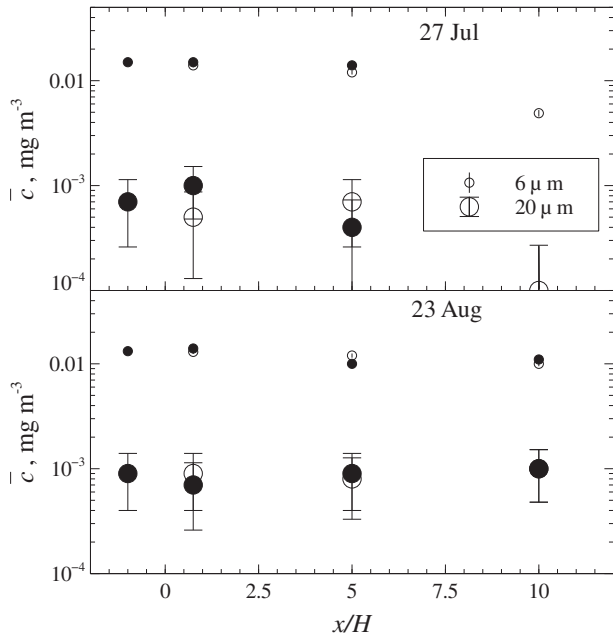


Fig. 4. Transects of 40 min mean particle concentration at height $z/H = 0.2$ on the reference transect (open symbols), and on the shelter transect (solid symbols), for particle size bins of width $\Delta d = 1 \mu\text{m}$ centred on diameters (6,20) μm . (Error bars, representing \pm one standard deviation, have been computed as $\bar{c}\sqrt{N}/N$, where N is the dust particle count and \bar{c} the inferred mean concentration.)

During the 40 min duration of an experiment any given sensor was exposed to the road dust clouds only during the repeated passages of the (twenty) individual clouds raised by the passing vehicle. Fig. 6 gives the first 420 s of the time series of instantaneous concentration observed by the Casella monitors on 23 Aug., and Fig. 7 gives the corresponding ensemble-averaged transient, formed by averaging all 20 realizations (c.f. Fig. 3 of Veranth et al., 2003; Fig. 3 of Etyemezian et al., 2004). According to Fig. 7 the “pulse area” or dosage, i.e. time integrated area under the ensemble mean concentration curve, is of order $10 \text{ mg s m}^{-3} \text{ trip}^{-1}$. Peak

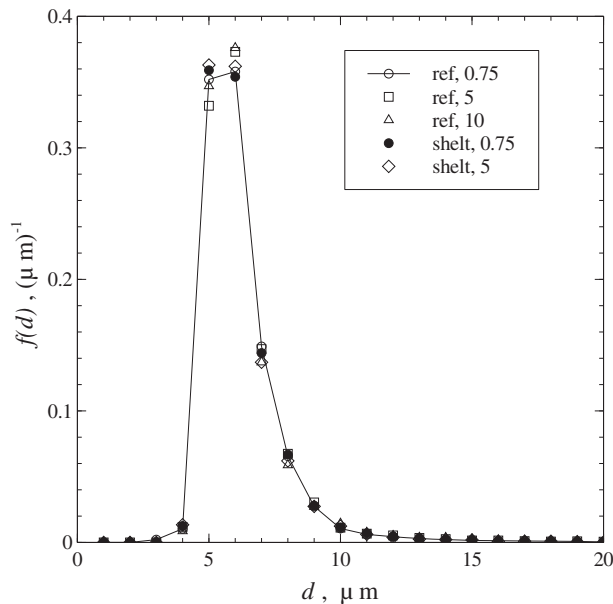


Fig. 5. Observed probability density function for dust diameter (27 July, 2011).

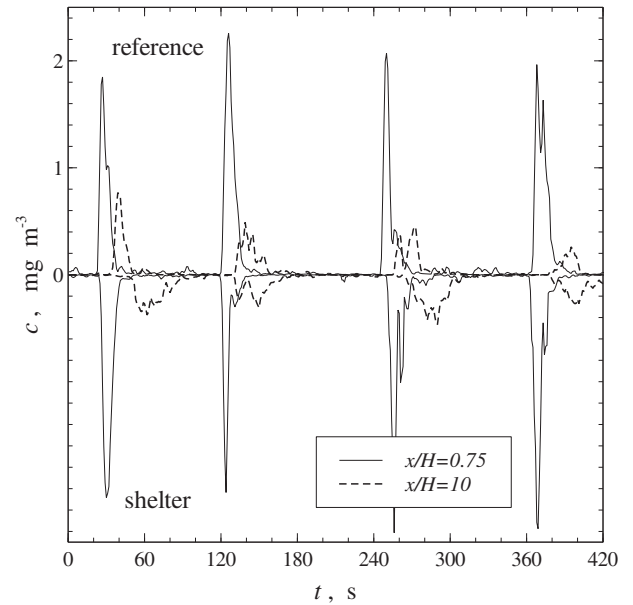


Fig. 6. Observed time series of dust concentration mg m^{-3} during the first four of twenty vehicle passes on 23 August 2011. A 3-point (3 s) block-average filter has been applied, and the sign of the observations on the shelter transect has been reversed.

values of concentration are of order 1 mg m^{-3} . (In forming these ensemble-averaged experimental concentration transients our assignment of the “time zero” points, when the vehicle should have been upwind of the transect, entailed an uncertainty that could amount to $\pm 5 \text{ s}$. Furthermore occasionally, and at random, a passing car raised a spurious cloud of dust. The impact of these complications must certainly have been to broaden the experimental concentration transients.)

At the location nearer to the road ($x/H = 0.75$) Figs. 6 and 7 indicate a substantial overlap (on the time axis) of the dust clouds in the open and in the lee of the shelterbelt, although in the wake of the trees the (ensemble mean) dust cloud dwelled longer

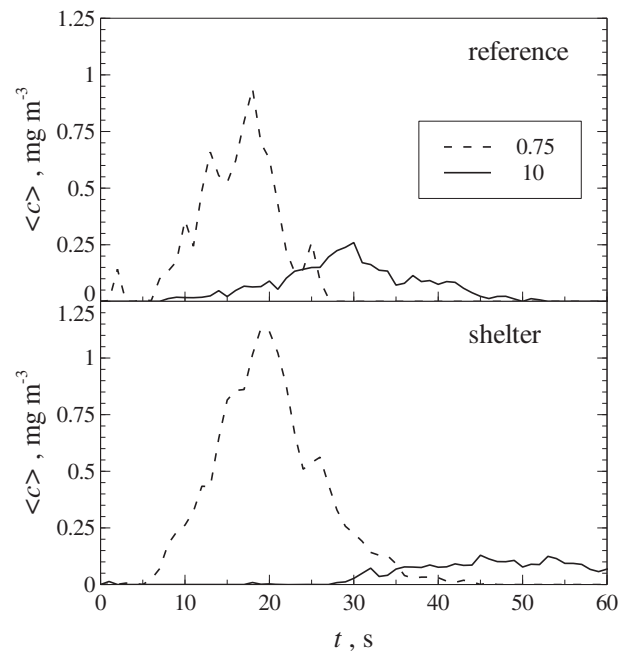


Fig. 7. Ensemble-averaged concentration transient, 23 August 2011.

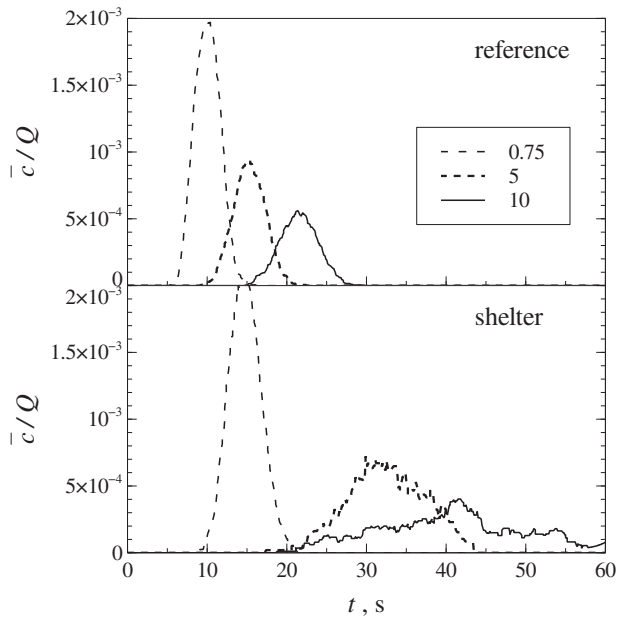


Fig. 8. Computed ensemble mean transients of normalized concentration for unsheltered (upper panel) and shelter flow. Transients are shown for $x/H=(0.75,5,10)$, where the coordinate origin is aligned at the centre of the shelterbelt (60 m or $6H$ downwind from the source of the dust).

over the instrument location. Farther downwind at $x/H = 10$ there is a clearer time-separation of the passing dust clouds on the reference transect and in the lee of the trees. Also apparent from Fig. 7 is the fact that the averaging of 20 transient clouds does not suffice to establish a smoothly varying ensemble mean transient. Many more realizations are needed – even in the neutrally-stratified conditions of these runs.

4.1. Simulation of the experiment

Fig. 8 gives the modelled concentration transients for $6 \mu\text{m}$ particles. There is some disparity relative to the observations (Fig. 7). Comparing first locations on the reference transect, at $x/H = 0.75$ observed and modelled dust clouds arrive at about the same time ($t \approx 5$ s), but the observed cloud dwells considerably longer over the detector. Farther downwind at $x/H = 10$ the core of the observed concentration transient appears approximately 10 s later than does that of the computed transient, perhaps a reflection of the fact that mean wind speed along the reference transect was in reality, and as shown by Fig. 3, slower than in the upwind region – a complication that would have retarded the arrival at $x/H = 10$ of the dust plume, and which was not represented in the LS model. The observed transient at $x/H = 10$ is furthermore some three times wider than that of the simulation, i.e. the real world dust clouds exhibit much wider alongwind spread. Turning now to the shelter transect, at $x/H = 0.75$ the arrival time of the model dust cloud is perhaps a few seconds late, and the cloud dwells over the detector for a much shorter interval than was observed. Only as regards the passage of the dust cloud over a detector at $x/H = 10$ downwind of the shelterbelt do the observed and modelled transients more or less coincide (however recall our earlier comment, see Section 4, as to a probable *spurious broadening* of the experimental concentration transients).

Accepting that the simulations are not in quantitative agreement with the observations as regards timing and duration of the concentration transients, we suggest that nevertheless it is not unreasonable to use the model *differentially*, to give an indication of the

effect of the shelterbelt. Fig. 9 gives (computed) concentrations averaged over the first 60 s after release, by which time all particles on the reference transect (and the great majority on the shelter transect) have been deposited, or have passed beyond $x/H = 15$. The computed mean concentration of $6 \mu\text{m}$ dust is *larger* in the lee of the shelterbelt than at the same location in the reference (undisturbed) winds. According to the calculation, then, and in contradiction of what has sometimes been supposed (i.e. that a shelterbelt “filters” the airstream), it would appear that a shelterbelt of the prescription modelled does not reduce the time-averaged concentration of PM_{10} road dust in the near downwind region.

4.2. Dust emission rate

The emission rate of dust from a road can be expressed in two unit systems. If the road is treated as an equivalent continuous line source, then we may assign an effective source strength Q having the unit $[\text{kg s}^{-1} \text{m}^{-1}]$; its numerical value must of course depend on the nature of the road surface and how that surface is *excited*, i.e. traffic volume, vehicle type and (perhaps) vehicle speed. An alternative quantification is to regard each unit of length of the road, upon being traversed by a single vehicle of a given type and at a given speed, as emitting a fixed quantity of dust mass – in which case the source strength (say, E) applies to a moving *instantaneous* point source (the latter is sometimes named an “emission factor” and its units are often cited in grams per vehicle kilometre traversed, g VKT^{-1}).

Under steady-state traffic conditions the two quantifications can be related as follows. Let $N[\text{m}^{-1}]$ denote the density of vehicles on the road, and $S[\text{m s}^{-1}]$ their speed. The flux of vehicles along the road is given by $NS[\text{s}^{-1}]$, and

$$Q = ENS \quad (15)$$

(where E has unit kg m^{-1}). To allow for different vehicle types and speeds, one may substitute a suitable summation for the right hand side. In the context of emissions promoted by repeated passages of a test vehicle, Gillies et al. (1999) relate Q to E by the formula

$$Q = E \frac{D}{TL} \quad (16)$$

where D/L is the ratio of the total vehicle-distance D covered (during the duration T of the test) to the length L of the test section, and equates to the number n of vehicle passes upwind of a transect (for Indian Head, $n = 20$ and $T = 40 \times 60$ s).

In experiments somewhat similar to ours Etyemezian et al. (2004) estimated E by time-height integration of the horizontal mass flux density measured on downwind towers,

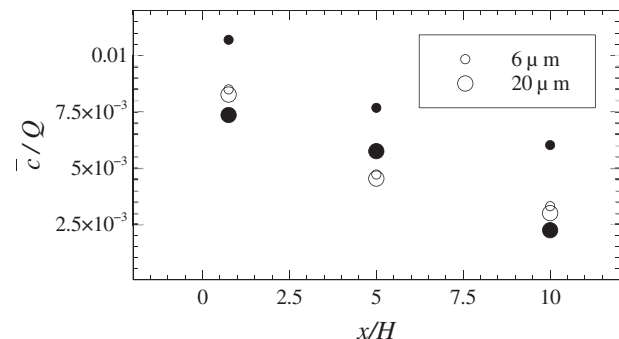


Fig. 9. Normalized mean concentration \bar{c}/Q at $z/H = 0.2$, averaged over the first 60 s after release of the dust cloud, as computed by the LS model. Open symbols, undisturbed winds; solid symbols, disturbed winds (as calculated by the RANS wind model, see Fig. 3).

$$E - \int_0^x D_0(x) dx = \int_{z=0}^{\infty} \int_{t=0}^{\infty} \bar{u}(z) \langle c(x, z, t) \rangle dz dt \quad (17)$$

where $D_0(x)$ is the deposition rate to ground. Etyemezian et al. used individual realizations $c(x, z, t)$ rather than the ensemble average $\langle c \rangle$ indicated above, but reported an “aggregate average over 116 passes” (of the vehicle). Their aggregate PM₁₀ fluxes at distances 7, 50 and 100 m downwind from the road differed by less than 10%, leading them to observe that deposition of PM₁₀ particles over a distance of up to 100 m from the unpaved road they studied was “too small to measure”.

The present experiment differs from earlier work (Gillies et al., 1999; Veranth et al., 2003; Etyemezian et al., 2004) in that the downwind dust flux density $\bar{u}\bar{c}$ was determined only at two heights, i.e. resolution did not permit to height-integrate the mass flux and estimate the flux off the road and its downstream depletion. We can, however, combine measurements of dust concentration at a single point with the particle trajectory simulation to infer the dust emission rate. The combination of a theoretical value \bar{c}_k/Q_k [s m⁻²] for the concentration at a point P of particles (of size class k) and a measured value \bar{c}_k [kg m⁻³] from a Rotorod at P allow to infer the size-specific emission rate Q_k [kg s⁻¹ m⁻¹], i.e. the equivalent strength of the road as a continuous line source. Taking for P the location $x/H = 0.75$ on the reference transect, and given that dust clouds had cleared this location within about 30 s, the 1 min mean values for \bar{c}_k/Q_k were multiplied by 20/40 (20 passes occupying 40 min). Table 3 gives the resulting apparent dust release rates, both as effective line source strength Q and as an emission factor E .

No particular significance can be attached to these estimated source strengths for the gravel road at Indian Head, nor should they necessarily be expected to be similar to source strengths from other roads, because the emission rate from unpaved roads is known to depend on numerous (generally uncontrolled and unknown) factors, including vehicle speed, weight and number of wheels, and the road surface silt content and moisture (Claiborn et al., 1995; Veranth et al., 2003). Veranth et al. estimated the PM₁₀ emission factor for a gravel road in a Utah desert by height-integrating the advective flux of dust immediately downwind of the road, and obtained numbers in the range of about 1000–4000 g VKT⁻¹. Claiborn et al. (1995, Table 4) tabulated PM₁₀ emission factors from unpaved roads in Spokane, Washington under uncontrolled but known traffic volumes, all but one of their estimates lying in the range 75–300 g VKT⁻¹. A comparable range of values was estimated by Kantamaneni et al. (1996, Table 5).

4.3. Impact of shelterbelt on suspended particle fraction

Table 4 gives the disposition of particles of several sizes, as computed by the trajectory model, one minute after their release

Table 3
Apparent equivalent line source strength [Q_k , mg s⁻¹ m⁻¹] and emission factor [E , g km⁻¹] of the gravel road at Indian Head, as excited by the test vehicle, for dust of various sizes (labelled k). These values were inferred as the ratio of the measured 40 min average concentration \bar{c}_k [kg m⁻³] at $x/H = 0.75$ on the reference transect to the theoretical ratio \bar{c}_k/Q_k [s m⁻²] given by the LS model for that same location.

$d, \mu\text{m}$	$Q_k^{\text{Jul. 27}}$	$Q_k^{\text{Aug. 23}}$	$E^{\text{Jul. 27}}$	$E^{\text{Aug. 23}}$
4	0.0075	0.011	0.9	1.4
5	0.55	0.48	66	58
6	0.80	0.75	85	90
7	0.55	0.47	66	57
8	0.32	0.28	38	34
9	0.21	0.21	26	25
10	0.10	0.11	13	14
20	0.033	0.06	4	7

Table 4

Computed fate of particles of several sizes, 60 s after their release from (near) the road surface, in undisturbed flow and in the shelter flow. From LS simulations with $u^* = 0.7 \text{ m s}^{-1}$, $z_0 = 0.03 \text{ m}$ ($U_r = 10.5 \text{ m s}^{-1}$).

	Undisturbed winds			Shelter flow		
	6, μm	20, μm	50, μm	6, μm	20, μm	50, μm
%Airborne	38	35	22	39.3	37	12
%Depos. ground	62	65	78	60.3	43	59
%Depos. foliage	–	–	–	0.4	20	29

near the road (note: recall that the Lagrangian stochastic model represents the profiles of velocity statistics on a grid, with vertical resolution 1 m. An LS model based on continuous profiles could be expected to provide slightly different numbers). In the undisturbed flow, 38% of 6 μm particles remain suspended one minute after release, a fraction that on first sight seems surprisingly low relative to the observation of Etyemezian et al. (2004) that loss of PM₁₀ between the road and a tower 100 m downwind was less than 9% (“at a downwind distance of 100 m, the removal of particles with aerodynamic diameter of 9.9 μm or less is not measurable”). Presumably the difference relates to the differing downwind surfaces of the present experiment and the desert surface of the Etyemezian et al. study.

However that may be, the goal of the present work was specifically to establish the effect of a shelterbelt on road dust dispersion. Table 4 indicates that, rather than exerting a helpful control over the finest and most predominant particles, the shelterbelt marginally increases the fraction of 6 μm particles remaining airborne after one minute. The absence of a decrease in airborne fraction can be explained by the small impaction conductance of 6 μm particles, but explaining an actual increase is not so simple. That increase has to be the result of a decreased fraction deposited on ground, which in turn implies a reduction in the 1 min averaged particle vertical velocity. Perhaps this reflects the influence of the mean updraft induced by the trees.

5. Conclusion

If shelterbelts are to be used to abate the problem of *fine* (PM₁₀ class) road dust, it appears that their character and/or their location will need to differ from that studied (a shelterbelt closer to the road would be liable to intercept and entrap a greater flux of the large particles that are susceptible to rapid gravitational settling, and should prove a more effective counter-measure). However the present finding, that a shelterbelt of the type (and in the location) investigated does not reduce the time-average concentration of fine road dust in the near downwind region, should be regarded as tentative. The field measurements alone are not sufficiently exhaustive and unambiguous to settle the matter, while the calculations entail several idealizations, namely, neglect or oversimplification of some aspects of the wind field (disturbance by the minor topography of roadside ditches; canopy and roughness sublayers; vehicle wake) and representation of the dust–shelterbelt interaction as a case of spheres intersecting uniform foliage having an arbitrary characteristic length scale of 0.05 m. In future work it would be helpful to expose many more dust sensors, sample many more plumes, isolate the reference (unsheltered) transects adequately from any influence of the shelter, and characterise the shelterbelt itself in much more detail. Another aspect needing to be established is the possible role of resuspension into the airstream of dust that had earlier been deposited onto foliage. The Indian Head shelterbelt did not appear dusty, but upwind-downwind measurements without road traffic would have clarified the question, and should be an aspect of future work.

Acknowledgements

We are grateful to two anonymous reviewers for their thoughtful and constructive suggestions. YM was supported during this research by the Student Research Affiliate Program at Agroforestry Development Centre, Agriculture and Agri-Food Canada.

References

- Bourdin, P., Wilson, J.D., 2008. Windbreak aerodynamics: is CFD reliable? *Boundary-Layer Meteorol.* 126, 181–208.
- Bouvet, T., Loubet, B., Wilson, J.D., Tuzet, A., 2007. Filtering of windborne particles by a natural windbreak. *Boundary-Layer Meteorol.* 123, 481–509.
- Claiborn, C., Mitra, A., Adams, G., Bamesberger, L., Allwine, G., Kantamaneni, R., Lamb, B., Westberg, H., 1995. Evaluation of PM₁₀ emission rates from paved and unpaved roads using tracer techniques. *Atmos. Environ.* 29, 1075–1089.
- Dyer, A.J., Bradley, E.F., 1982. An alternative analysis of flux-gradient relationships at the 1976 ITCE. *Boundary-Layer Meteorol.* 22, 3–19.
- Etyemezian, V., Ahonen, S., Nikolic, D., Gillies, J., Kuhns, H., Gillette, D., Veranth, J., 2004. Deposition and removal of fugitive dust in the arid southwestern United States: measurements and model results. *J. Air Waste Manage. Assoc.* 54, 1099–1111.
- Gillies, J.A., Watson, J.G., Rogers, C.F., DuBois, D., Chow, J.C., Langston, R., Sweet, J., 1999. Long-term efficiencies of dust suppressants to reduce PM₁₀ emissions from unpaved roads. *J. Air Waste Manage. Assoc.* 49, 3–16.
- Kantamaneni, R., Adams, G., Bamesberger, L., Allwine, E., Westberg, H., Lamb, B., Claiborn, C., 1996. The measurement of roadway PM₁₀ emission rates using atmospheric tracer ratio techniques. *Atmos. Environ.* 30, 4209–4223.
- Launder, B., Reece, G., Rodi, W., 1975. Progress in the development of a Reynolds-Stress turbulence closure. *J. Fluid Mech.* 68, 537–566.
- Paulson, C.A., 1970. The mathematical representation of wind speed and temperature profiles in the unstable atmospheric surface layer. *J. Appl. Meteorol.* 9, 857–861.
- Pardyjak, E.R., Speckart, S.O., Yin, F., Veranth, J.M., 2008. Near source deposition of vehicle generated fugitive dust on vegetation and buildings: model development and theory. *Atmos. Environ.* 42, 6442–6452.
- Peltola, H., Nykänen, M.-L., Kellomäki, S., 1997. Model computations on the critical combination of snow loading and windspeed for snow damage of scots pine, Norway spruce and Birch sp. at stand edge. *For. Ecol. Manag.* 95, 229–241.
- Raupach, M.R., Woods, N., Dorr, G., Leys, J.F., Cleugh, H.A., 2001. The entrapment of particles by windbreaks. *Atmos. Environ.* 35, 3373–3383.
- Steffens, J.T., Wang, Y.J., Zhang, K.M., 2012. Exploration of effects of a vegetation barrier on particle size distributions in a near-road environment. *Atmos. Environ.* 50, 120–128.
- Veranth, J.M., Pardyjak, E.R., Seshadri, G., 2003. Vehicle-generated fugitive dust transport: analytic models and field study. *Atmos. Environ.* 37, 2295–2303.
- Wilson, J.D., 1985. Numerical studies of flow through a windbreak. *J. Wind Eng. Ind. Aero.* 21, 119–154.
- Wilson, J.D., 2000. Trajectory models for heavy particles in atmospheric turbulence: comparison with observations. *J. Appl. Meteorol.* 39, 1894–1912.
- Wilson, J.D., 2004. Oblique, stratified winds about a shelter fence, II: comparison of measurements with numerical models. *J. Appl. Meteorol.* 43, 1392–1409.
- Wilson, J.D., Yee, E., Ek, N., d'Amours, R., 2009. Lagrangian simulation of wind transport in the urban environment. *Q. J. R. Met. Soc.* 135, 1586–1602 (See also erratum, *Q. J. R. Met. Soc.*, 136, 552, January 2010).
- Wilson, J.D., Flesch, T.K., Bourdin, P., 2010. Ground-to-air gas emission rate inferred from measured concentration rise within a disturbed atmospheric surface layer. *J. Appl. Meteorol. Climatol.* 49, 1818–1830.